Electronic supplementary information for

Nitric oxide generation activity from unsymmetrical β-diketiminato copper(II) nitrite complexes

Kuldeep Chand,[a] Yu-Cheng Chu,[a] Tzai-Wei Wang,[c] Chai-Lin Kao,[a] Ya-Fan Lin,[a, b*] Ming-Li Tsai,[a,c*] Sodio C. N. Hsu[a,c,d*]

[a]*Department of Medicinal and Applied Chemistry, Drug Development and Value Creation Research Center, Kaohsiung Medical University, Kaohsiung 807, Taiwan*

[b]*Department of Fragrance and Cosmetic Science, Kaohsiung Medical University, Kaohsiung 807, Taiwan*

[c]*Department of Chemistry, National Sun Yat-Sen University, Kaohsiung 804, Taiwan.*

[d]*Department of Medical Research, Kaohsiung Medical University Hospital, Kaohsiung 807, Taiwan.*

Contents

Fig. S10 ^{31}P NMR spectrum (400 MHz, C$_6$D$_6$) of **L$_1$**Cu(O$_2$N) with two equivalents of PPh$_3$.

Fig. S11 ^{31}P NMR spectrum (400 MHz, C$_6$D$_6$) of **L$_1$**Cu(O$_2$N) with three equivalents of PPh$_3$.

Fig. S12 ^{31}P NMR spectrum (400 MHz, C$_6$D$_6$) of **L$_2$**Cu(O$_2$N) with two equivalents of PPh$_3$.

Fig. S13 ^{31}P NMR spectrum (400 MHz, C$_6$D$_6$) of **L$_2$**Cu(O$_2$N) with three equivalents of PPh$_3$.

Fig. S14 UV-Vis. spectra (in CH$_2$Cl$_2$ at 25 °C) of (TPP)Co (Black trace) and (TPP)Co(NO) species generated upon reacting (TPP)Co with NO released from the mixture of **L$_1$**Cu(O$_2$N)(blue), **L$_2$**Cu(O$_2$N)(red) and PPh$_3$.

Fig. S15 a) UV-vis spectra showing the shift in absorbance band of cobalt(II) porphyrin (TPP)Co(II) (TPP= tetraphenylporphyrin) with increasing level of complexation to NO. b) Calibration curve extracted from the peak maxima, showing the linear trend in absorption maximum shift with % complexation to NO. The spectra show **L$_1$**Cu(O$_2$N) (red) and **L$_2$**Cu(O$_2$N) (blue).

Fig. S16 CV diagrams of **L$_1$**Cu(O$_2$N) (a) and **L$_2$**Cu(O$_2$N) (b) after PPh$_3$ addition.

Fig. S17 CV diagram of dissolved NO(g) with various concentration in CH$_3$CN solution.

Fig. S18 Standardization plot of NO(g).

Fig. S19 Reaction of **L$_1$**Cu(O$_2$N) with excess of PPh$_3$ (25~50 equivalents) in CH$_2$Cl$_2$ at 25 °C.

Fig. S20 Reaction of **L$_1$**Cu(O$_2$N) with excess of PPh$_3$ (25~50 equivalents) in CH$_2$Cl$_2$ at 25 °C.

Fig. S21 Eyring plot for the reaction of **L$_1$**Cu(O$_2$N) with two equivalents of PPh$_3$.

Fig. S22 Eyring plot for the reaction of **L$_2$**Cu(O$_2$N) with two equivalents of PPh$_3$.

Table S1 The experimental and calculated metric parameters of **L$_1$**CuCl and **L$_2$**CuCl.

Table S2 The overlap population analysis between Cu and coordinated donor atoms for the β-LUMOs of **L$_1$**CuCl and **L$_2$**CuCl.

Table S3 First order rate constants for reaction of copper(II) nitrito complexes (2 mM) with triphenyl-phosphine (4 mM) in CH$_2$Cl$_2$ at 278-308 K.

Table S4 Values of $E_{1/2}$ for Cu(II) complexes.

Table S5 DFT optimized result: atomic coordinates of **L$_1$**CuCl.

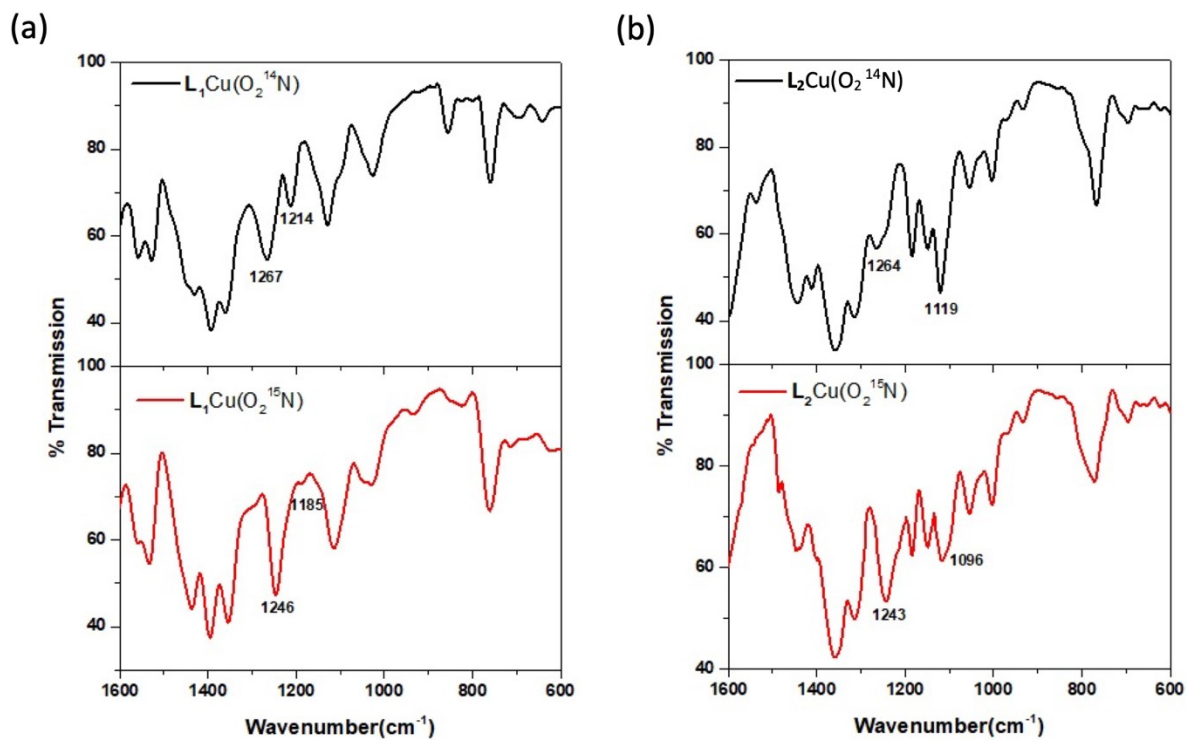**Table S6** DFT optimized result: atomic coordinates of **L$_2$**CuCl.

Fig. S1. (a) FT-IR spectra (KBr pellet) of complexes $L_1Cu(O_2{}^{14}N)$ (black) with $L_1Cu(O_2{}^{15}N)$ (red) and (b) $L_2Cu(O_2{}^{14}N)$ (black) with $L_2Cu(O_2{}^{15}N)$ (red).

(a) — $L_1Cu(O_2N)$ -0.099 V   -0.255 V   E(V) vs SCE

(b) — $L_2Cu(O_2N)$ +0.194 V   +0.059 V   E(V) vs SCE
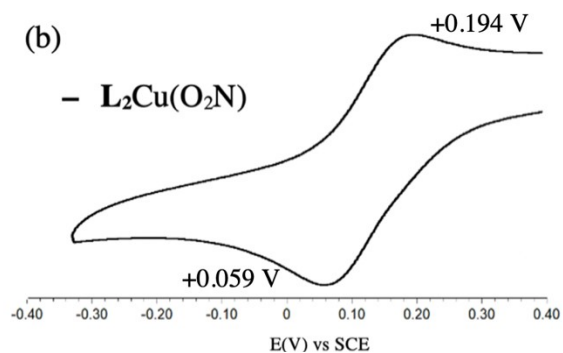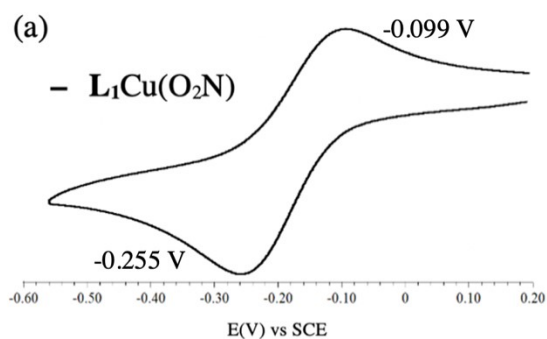
Fig. S2 CV diagrams of L_1CuCl (a), L_2CuCl (b), L_3CuCl (c), and L_4CuCl (d) in MeCN (1×10^{-3} M). Scan rate = 300 mV s^{-1}, electrolyte = (Bu_4N) (PF_6) (0.1 M). Note: Potentials are vs SCE (Ferrocene/Ferrocenium couple in CH$_3$CN solution, $E_{1/2}$ = + 400 mV).

(a) — L_1CuCl -0.092 V   -0.240 V   E(V) vs SCE

(b) — L_2CuCl +0.140 V   -0.032 V   E(V) vs SCE

(c) — L_3CuCl -0.152 V   -0.362 V   E(V) vs SCE

(d) — L_4CuCl +0.060 V   -0.142 V   E(V) vs SCE
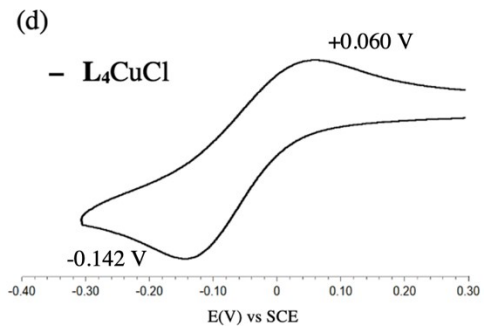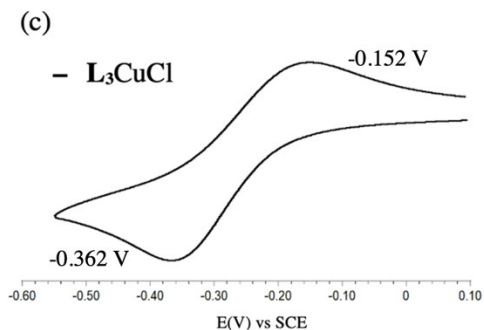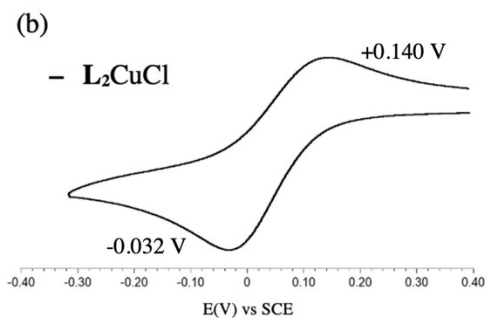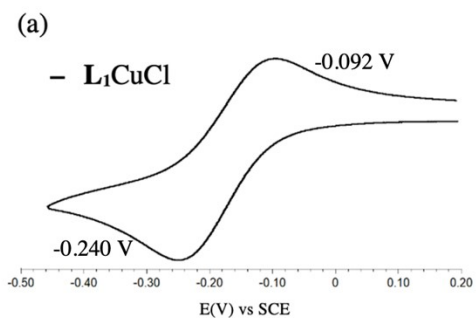
Fig. S3 CV diagrams of **L₁**Cu(O₂N) (a) and **L₂**Cu(O₂N) (b) in MeCN (1×10⁻³ M). Scan rate = 300 mV s⁻¹, electrolyte = (Bu₄N)(PF₆) (0.1 M). Note: Potentials are vs SCE (Ferrocene/Ferrocenium couple in CH₃CN
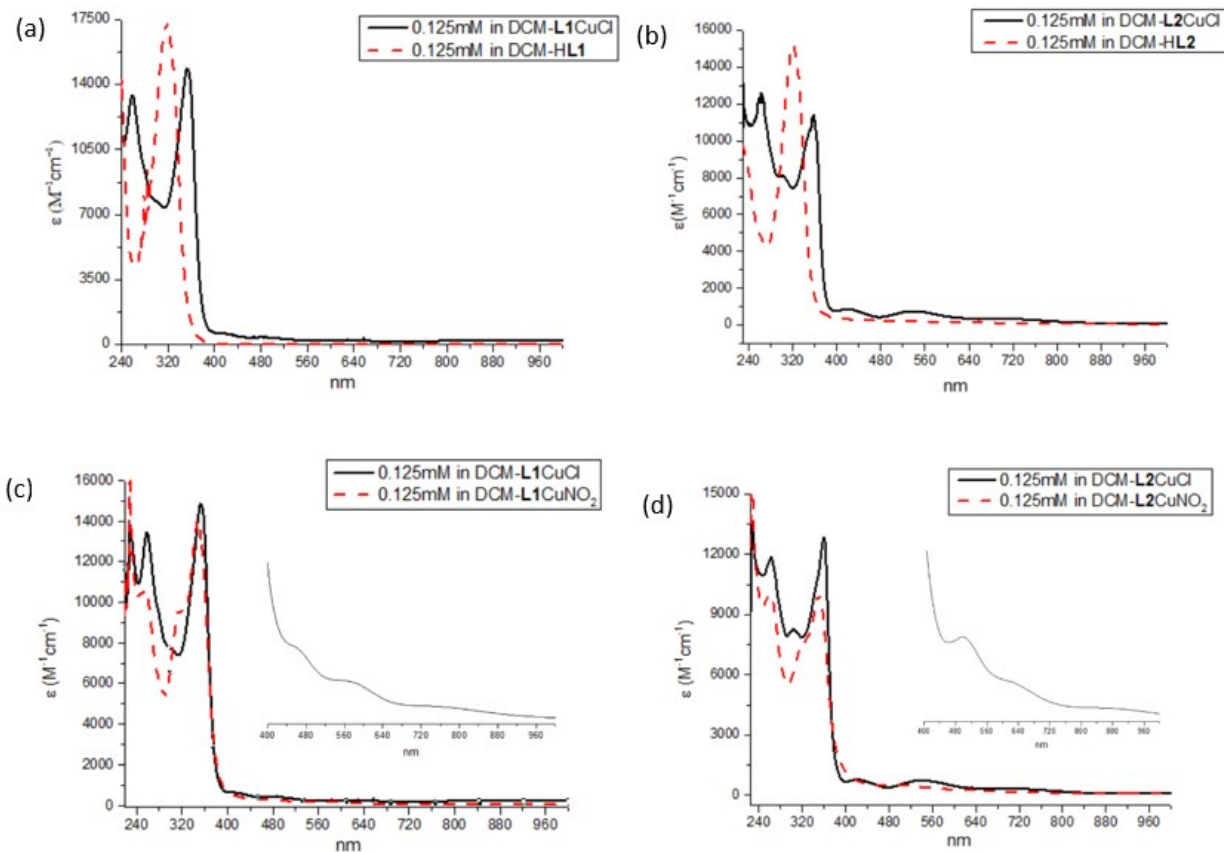
solution, $E_{1/2}$ = + 400 mV).

Fig. S4. Absorption spectra of complexes **L₁**CuCl (a), **L₂**CuCl (b) and **L₁**Cu(O₂N) (c), **L₂**Cu(O₂N) (d) in CH₂Cl₂ at room temperature.
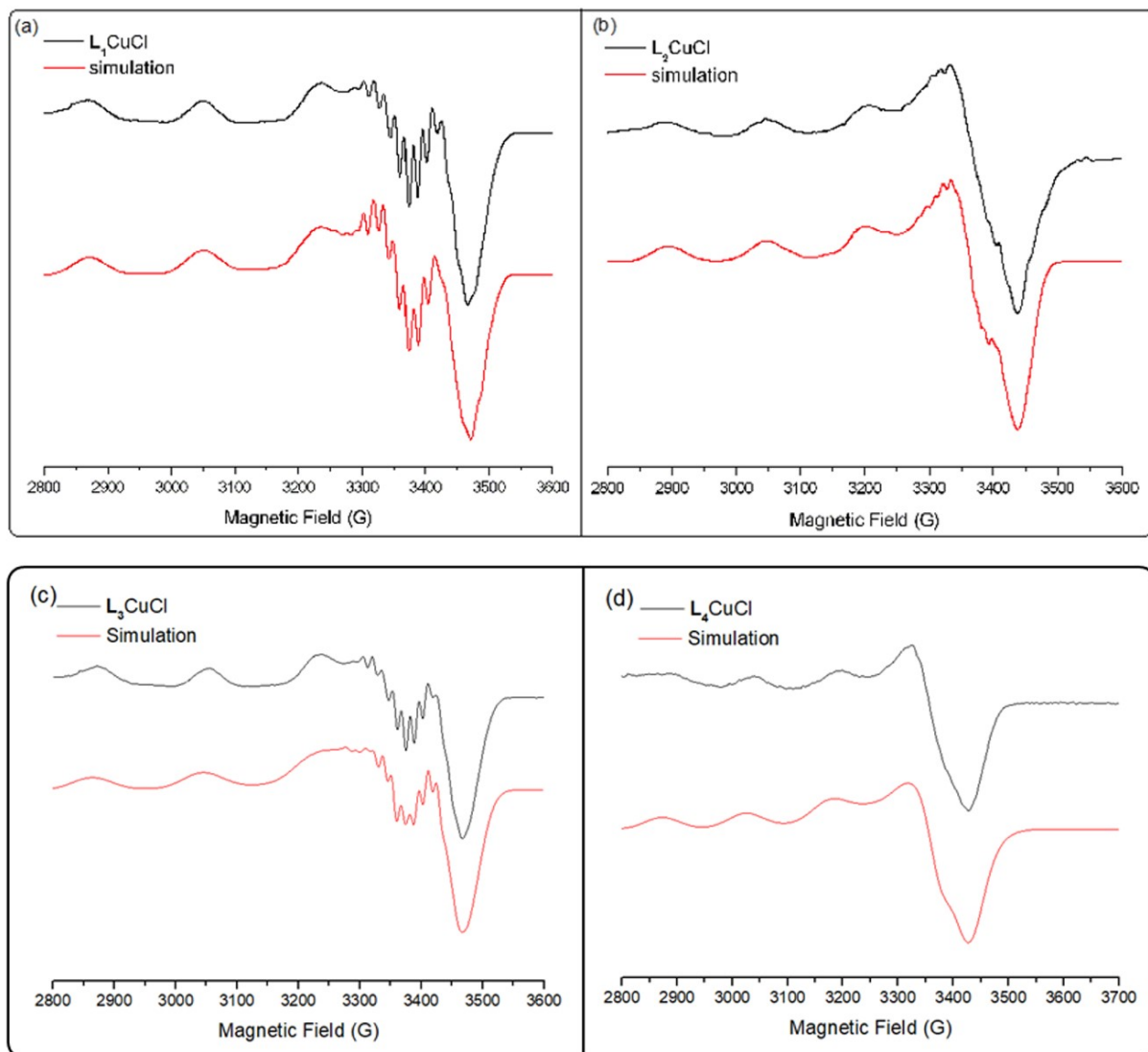
Fig. S5 Experimental (black) and simulated (red) EPR spectra of **L₁**CuCl (a), **L₂**CuCl (b), **L₃**CuCl (c), and **L₄**CuCl (d).
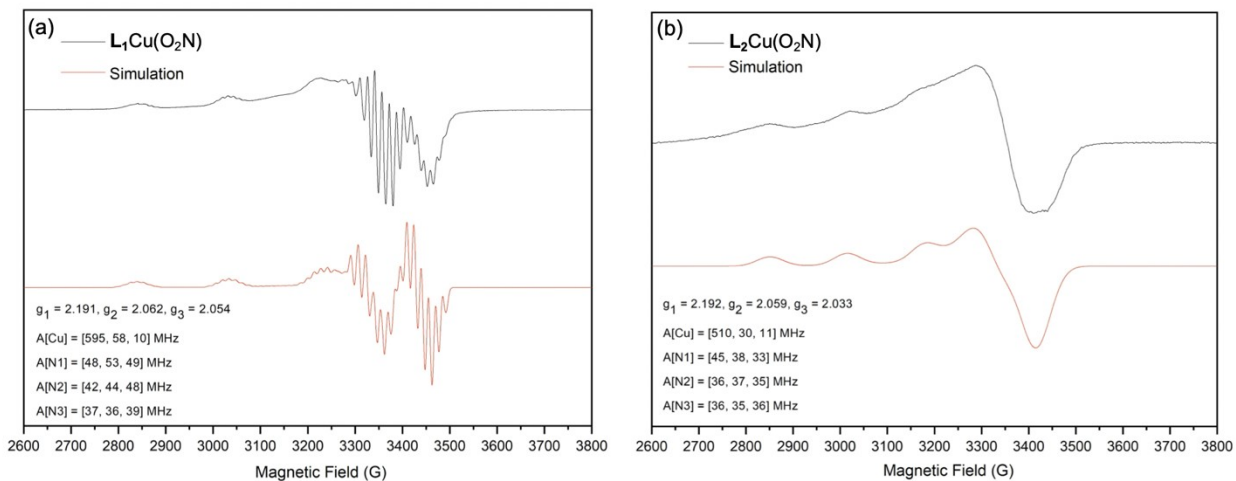
Fig. S6 Experimental (black) and simulated (red) EPR spectra of $L_1Cu(O_2N)$ (a) and $L_2Cu(O_2N)$ (b). Note that the linewidth of simulation spectrum of $L_1Cu(O_2N)$ was modeled by a combination of linewidth broaden function [3, 3, 2] MHz, g-strain [0.003, 0.002, 0.0028], and A-strain [2, 1.5, 1] MHz; the linewidth of simulation spectrum of $L_2Cu(O_2N)$ was modeled by a combination of linewidth broaden function [3, 3, 2] MHz, g-strain [0.018, 0.018, 0.018], and A-strain [2, 1.5, 1] MHz.
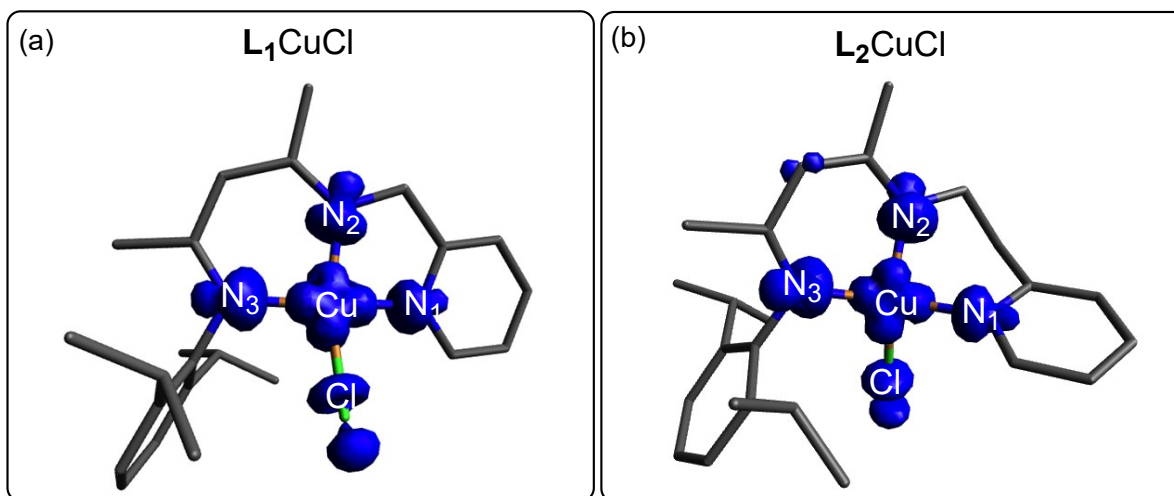
Fig. S7 The spin density distributions of L_1CuCl (a) and L_2CuCl (b).
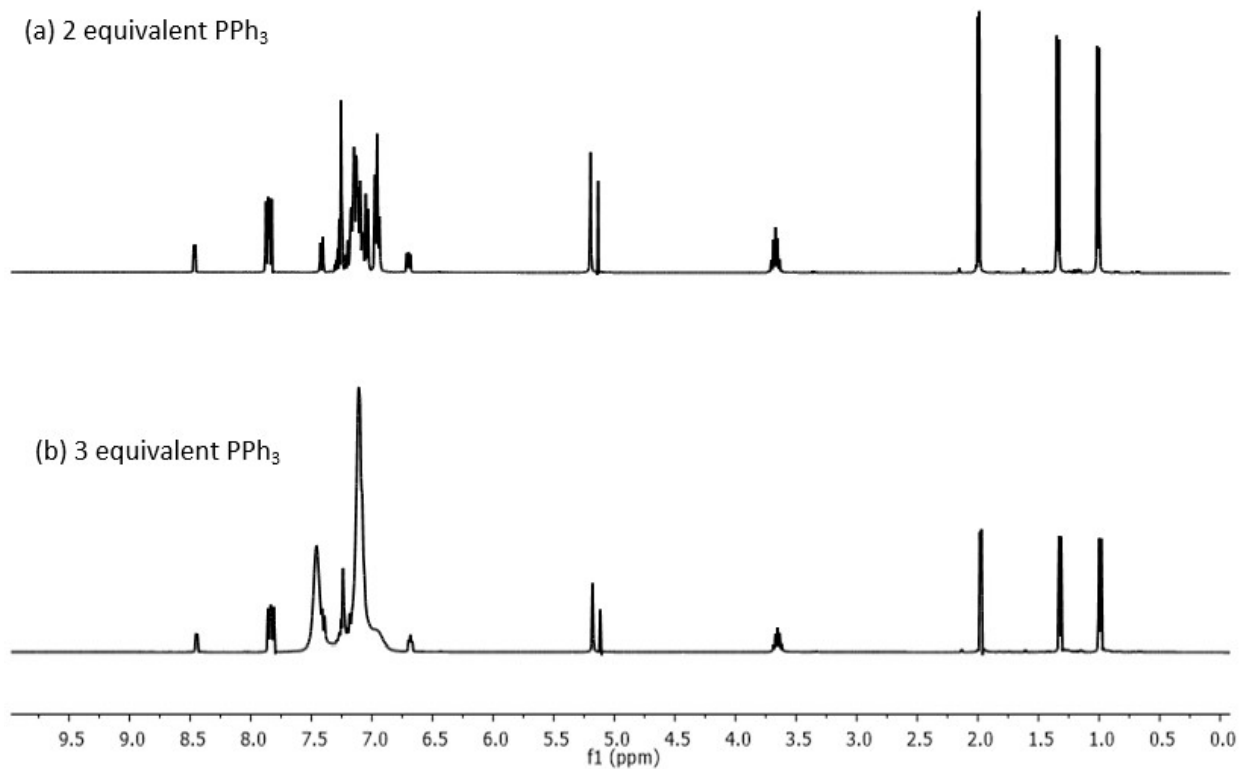
Fig. S8 Comparison of ^{1}H NMR spectrum (400 MHz, C_6D_6) of **L₁Cu(O₂N)** with (a) two and (b) three equivalents of PPh₃.
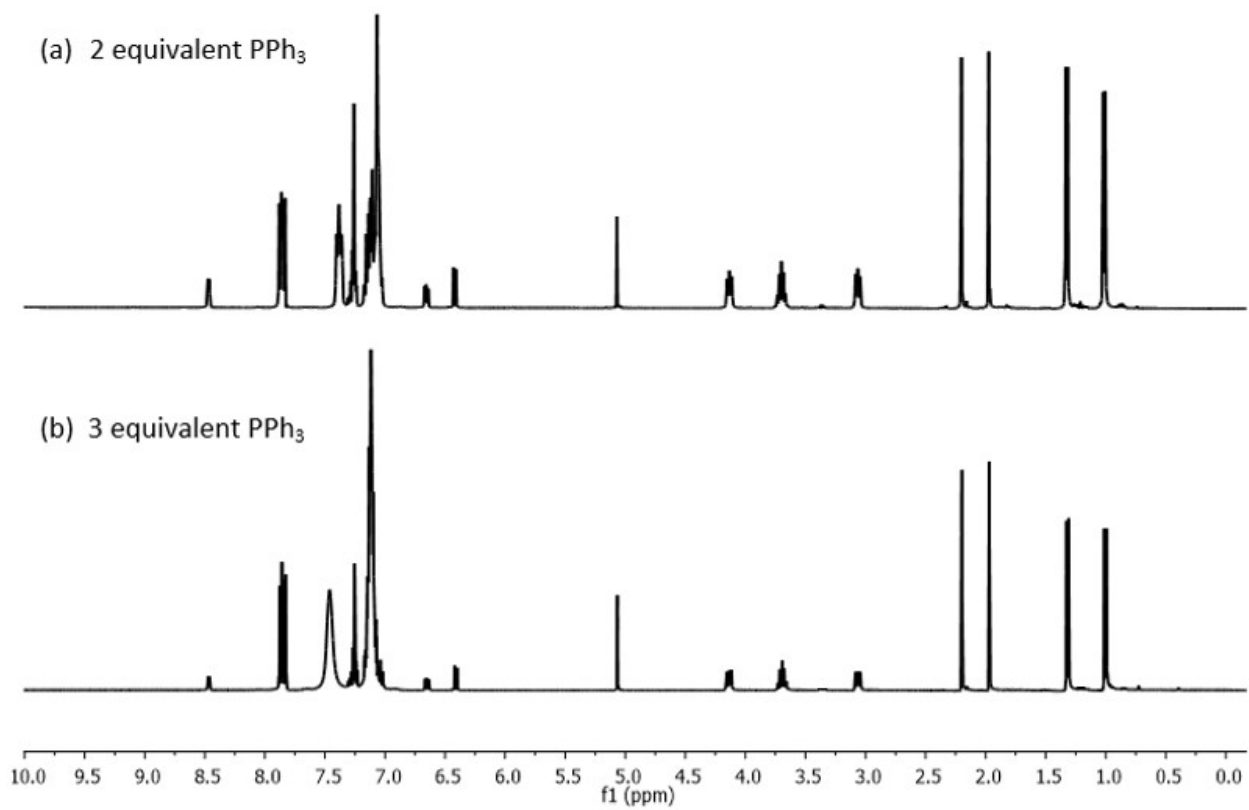
Fig. S9 Comparison of ^{1}H NMR spectrum (400 MHz, C_6D_6) of **L₂Cu(O₂N)** with (a) two and (b) three equivalents of PPh₃.
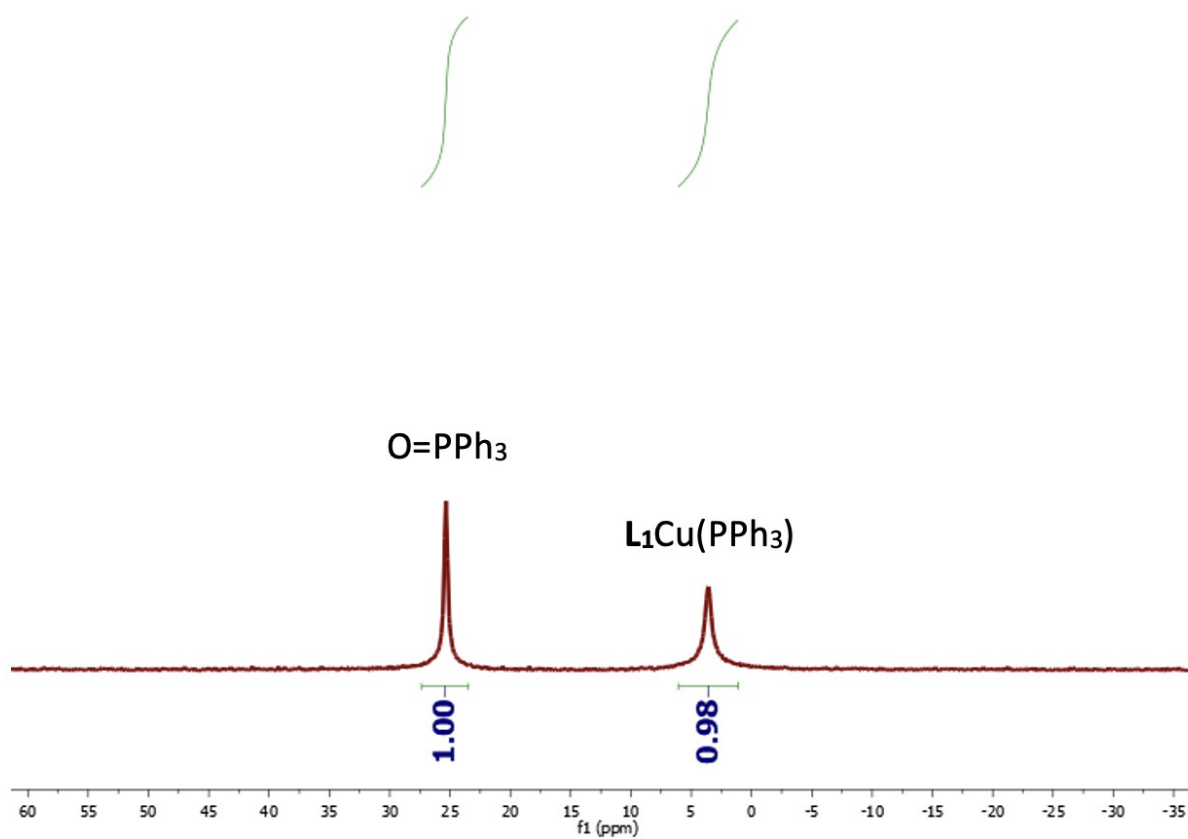
Fig. S10 ^{31}P NMR spectrum (400 MHz, C_6D_6) of **L$_1$Cu(O$_2$N)** with two equivalents of PPh$_3$.
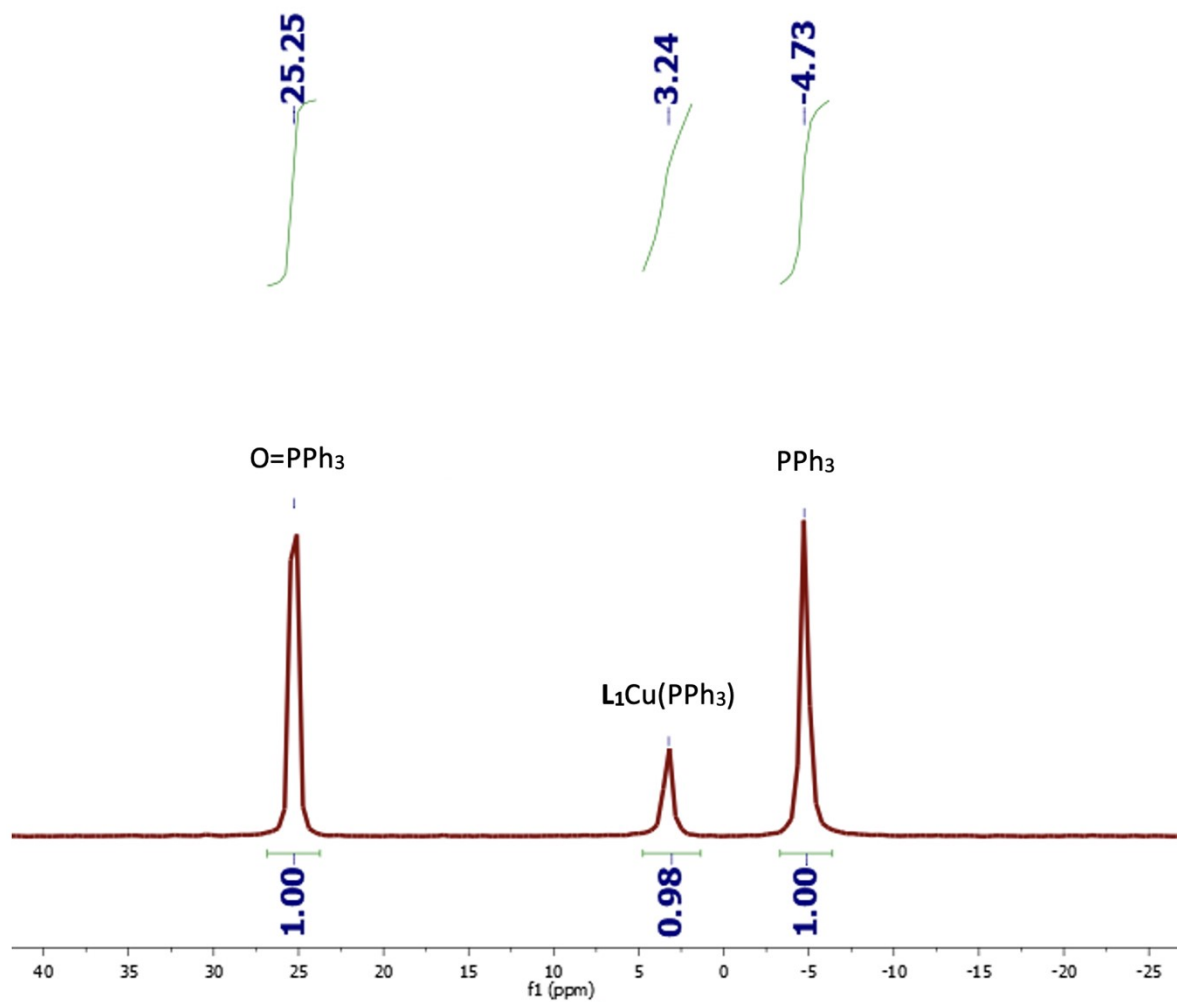
Fig. S11 ^{31}P NMR spectrum (400 MHz, C$_6$D$_6$) of **L$_1$Cu(O$_2$N)** with three equivalents of PPh$_3$.
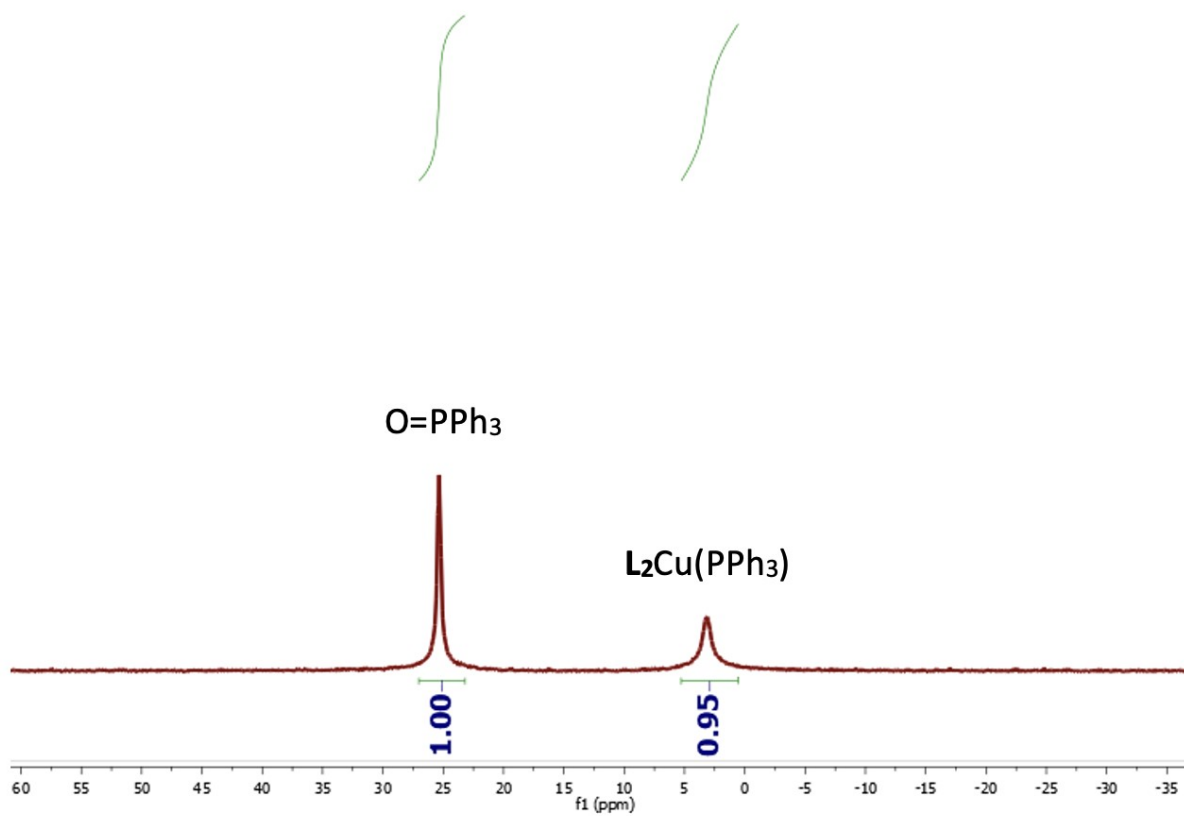
Fig. S12 ^{31}P NMR spectrum (400 MHz, C_6D_6) of **L₂Cu(O₂N)** with two equivalents of PPh₃.
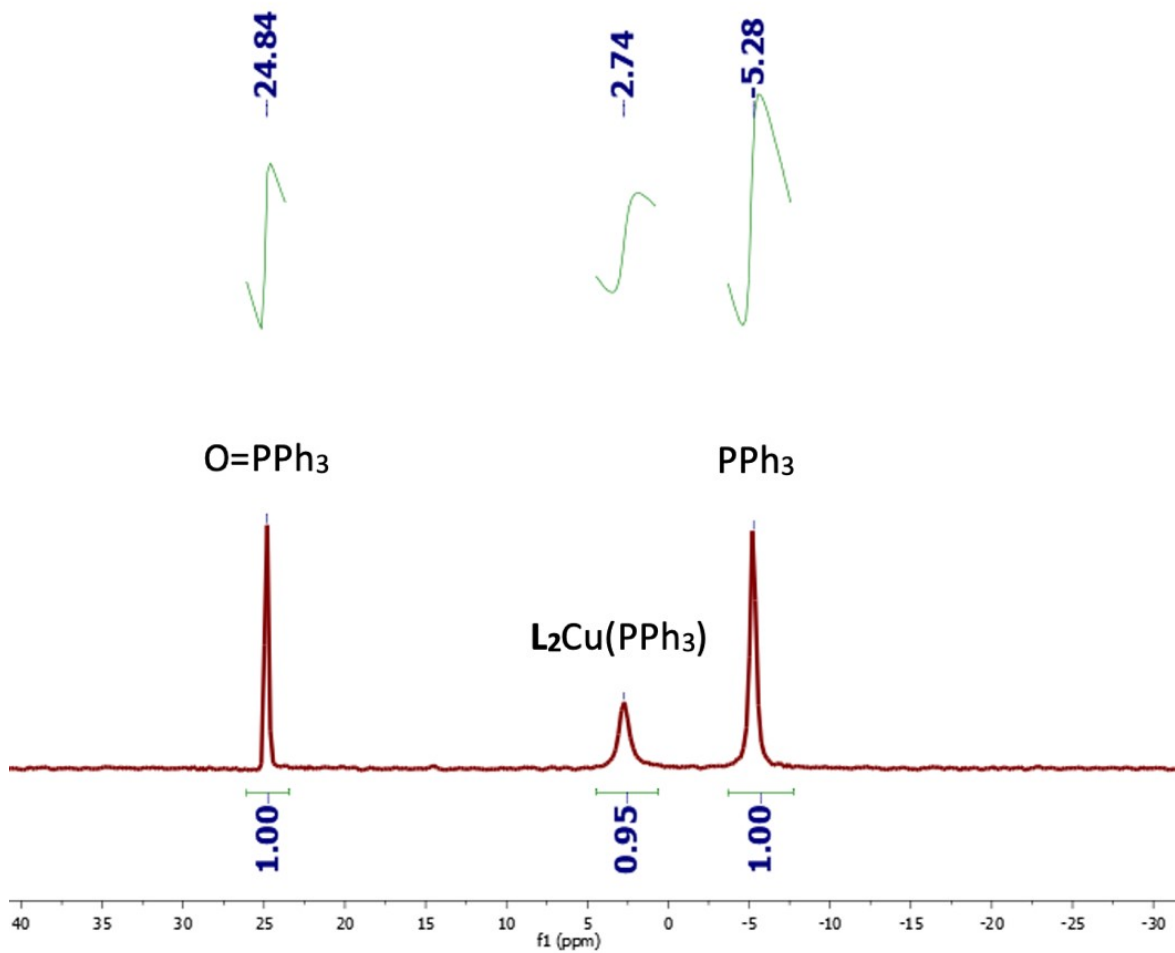
Fig. S13 ^{31}P NMR spectrum (400 MHz, C_6D_6) of **L$_2$Cu(O$_2$N)** with three equivalents of PPh$_3$.

Quantitative NO release by (TPP)Co(II) complexes: Nitric oxide production was quantified similarly to previously published procedures.[1-7] A solution of $L_1Cu(O_2N)$ (9.16 mg, 20 mmol) or $L_2Cu(O_2N)$ (9.44 mg, 20 mmol) in dichloromethane (1 mL) was prepared in a small vial capped with a rubber septum. A solution of PPh_3 (10.5 mg, 80 mmol) in dichloromethane (0.5 mL) was then introduced with a syringe at room temperature. The solution leads to gradual color change from dark brown $L_1Cu(O_2N)$ and green $L_2Cu(O_2N)$ to yellow within 5 minutes. Trapping of the evolved gas with the cobalt(II) porphyrin (TPP)Co(II) (TPP= tetraphenylporphyrin) leads to the formation of the corresponding complex (TPP)Co(NO) indicating a clear stochiometric reduction of nitrite to NO in presence of PPh_3. NO is released in 91 % and
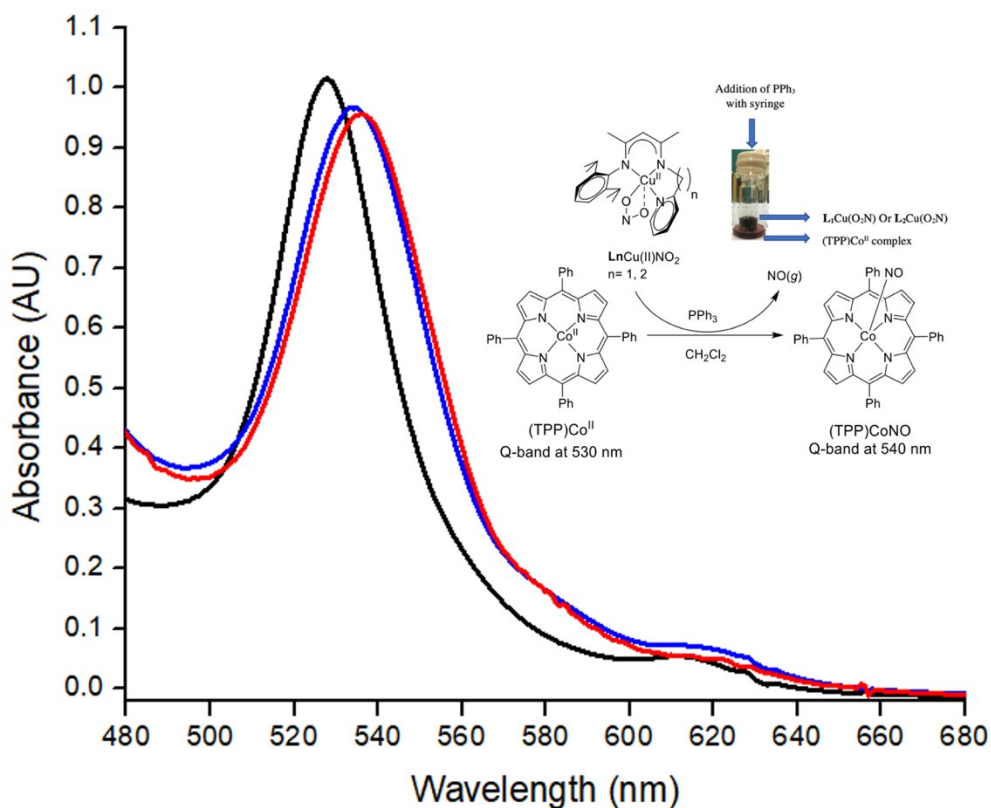
81% yield in case of $L_1Cu(O_2N)$ and $L_2Cu(O_2N)$ as measured by gas trapping experiment respectively.

Fig. S14 UV-Vis. spectra (in CH$_2$Cl$_2$ at 25 °C) of (TPP)Co (Black trace) and (TPP)Co(NO) species generated upon reacting (TPP)Co with NO released from the mixture of **L$_1$**Cu(O$_2$N) (red), **L$_2$**Cu(O$_2$N)
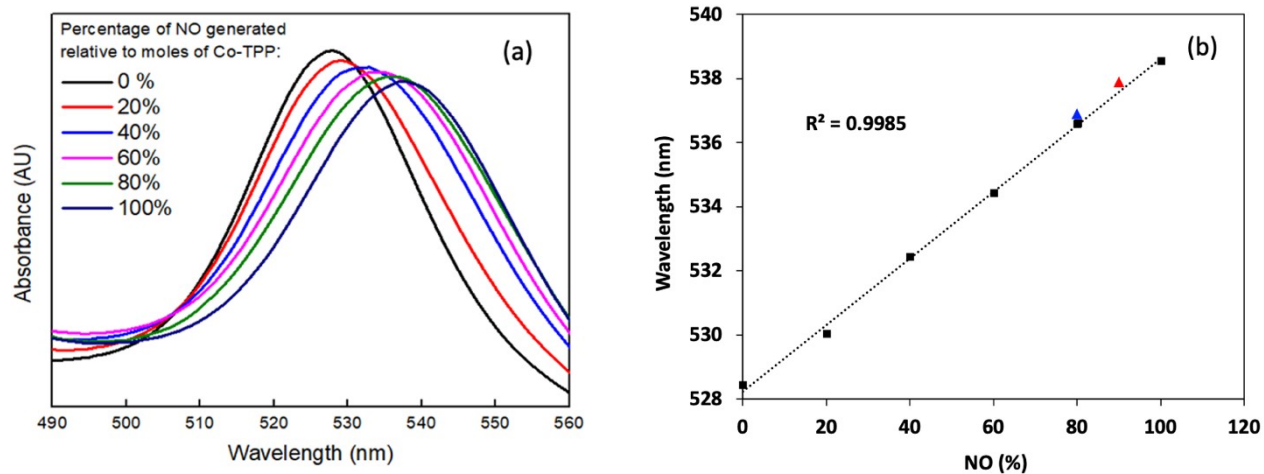
(blue) and PPh$_3$.

Fig. S15 a) UV-vis spectra showing the shift in absorbance band of cobalt(II) porphyrin (TPP)Co(II) (TPP= tetraphenylporphyrin) with increasing level of complexation to NO. b) Calibration curve extracted from the peak maxima, showing the linear trend in absorption maximum shift with % complexation to NO. The spectra show **L$_1$**Cu(O$_2$N) (red) and **L$_2$**Cu(O$_2$N) (blue).[7]
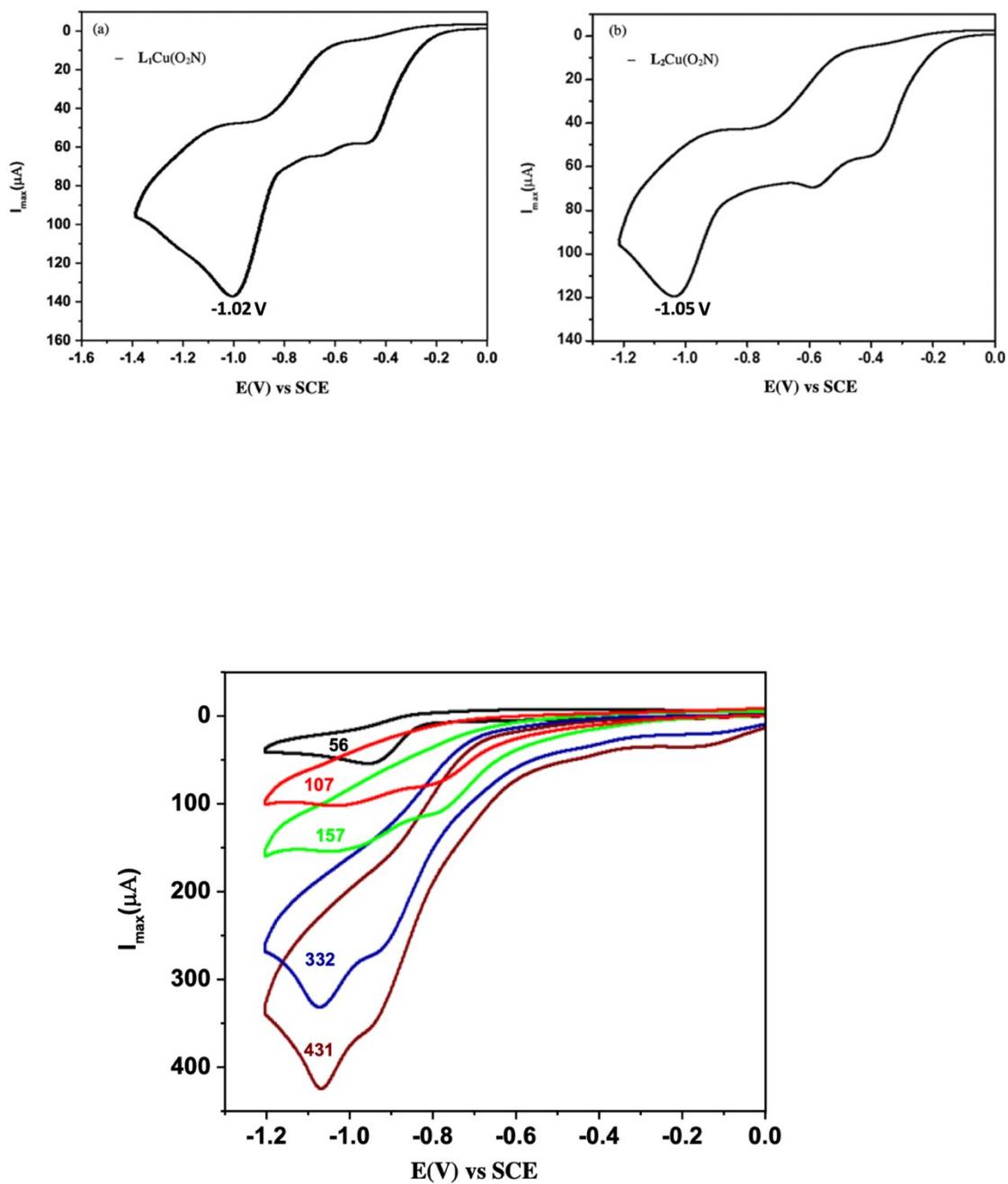
Fig. S16 CV diagrams in MeCN (1×10^{-3} M) at scan rate = 300 mV s^{-1} using electrolyte = $(Bu_4N)(PF_6)$ (0.1 M). $L_1Cu(O_2N)$ (a) and $L_2Cu(O_2N)$ (b) gradually developed -1.02~1.05 V response upon reduction, followed by PPh$_3$ addition.

Note: Potentials are vs SCE (Ferrocene/Ferrocenium couple in CH$_3$CN solution, E$_{1/2}$ = + 400 mV).

Fig. S17 CV of NO dissolved in 20 mL CH_3CN solution containing $(Bu_4N)(PF_6)$ as supporting electrolyte
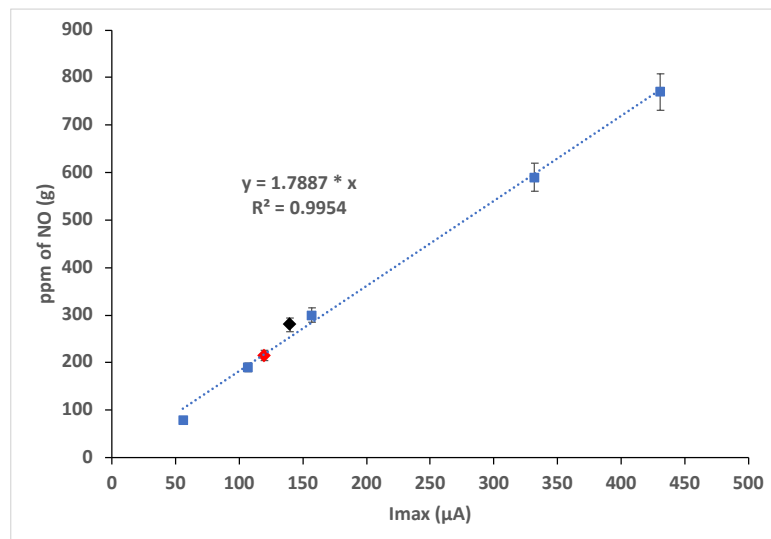
at 298 K at a glassy-carbon working electrode at a scan rate of 300 mV s^{-1} using Ferrocene/Ferrocenium as reference electrode: [NO] are 0.7 ml (56 ppm), 1.5 ml (107 ppm), 3ml (157 ppm), 5 ml (332 ppm) and 7 ml (431 ppm); maximum ipc observed electrochemically are 79, 190, 300, 590 and 770 respectively.[1, 2]

Note: Potentials are vs SCE (Ferrocene/Ferrocenium couple in CH_3CN solution, $E_{1/2} = + 400$ mV).

Fig. S18 Standardization plot of [NO(g)]. The ppm of NO for complexes $L_1Cu(O_2N)$ (black) and $L_2Cu(O_2N)$ (red) has been presented.

Calculation for liberated NO(g) from reaction of reduced $L_1Cu(O_2N)$ in 20 mL CH_3CN with PPh_3:

Imax(μA) obtained at - 0.97 V (the reduced CH_3CN solution of $L_1Cu(O_2N)$ (0.98 mmol) + PPh_3) = 135 (Fig. S4a). From the slope of the calibration plot (Fig. S6) this Imax correspond to 1.788 x 135 = 241.38 ppm of NO(g) that is liberated from a 0.98 mmol CH_3CN solution (20 mL) of reduced $L_1Cu(O_2N)$.

F.Wt. of $L_1Cu(O_2N)$ = 458.07

458.07 mg of $L_1Cu(O_2N)$ in 1L CH_3CN = 30 gm of NO(g) in 1 L = 3 x 10^4 ppm of NO(g) [1 ppm = 1 mg/L], Therefore (458.07 x 20) / 1000 mg i.e., 9.16 mg of $L_1Cu(O_2N)$ in 20 mL = (30 x 20) / 1000 mg i.e., 0.45 mg NO(g) in 20 mL = 30 ppm NO(g) = 100% NO(g) evolution

9.0 mg of $L_1Cu(O_2N)$ is dissolved in 20 mL of CH_3CN (0.98 mmol) = (30 x 9.0) / 9.16 i.e., 29.47 * 3 = 88.41 ppm NO(g) for 100% NO(g) evolution.

If 88.41 ppm NO(g) liberates then it will be 100% NO(g) evolution, however the liberated amount of NO(g) is 241.38
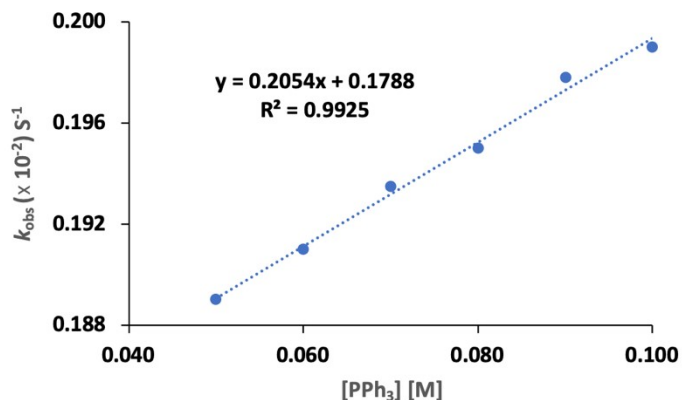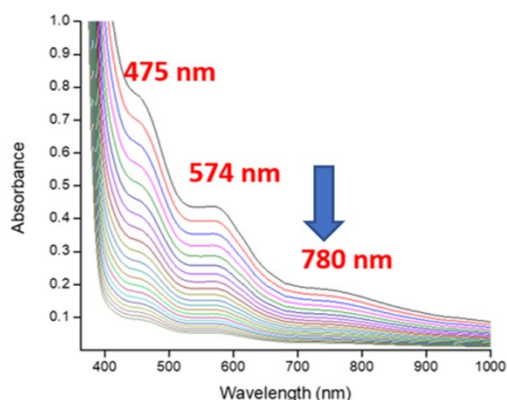
ppm. Therefore yield % NO(g) evolution = (241.38 x 100) / 88.41 = 273.02 / 3 = 91 ± 1.45 %

After similar calculation for $L_2Cu(O_2N)$ the NO release yield was found to be 81 ± 0.32 %.

Note: A three times higher concentration of $L_1Cu(O_2N)$ and $L_2Cu(O_2N)$ has been used in the experiment for calibration
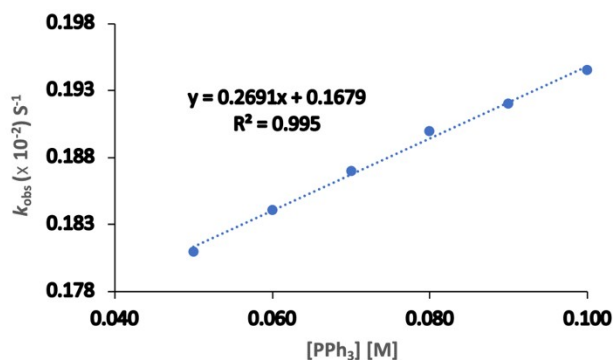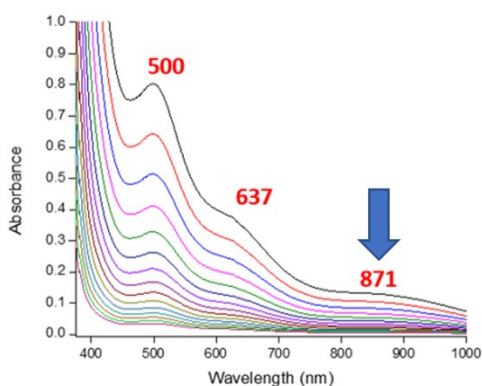
curve (Fig. S6).

Fig. S19 Reaction of $L_1Cu(O_2N)$ with excess of PPh_3 (25~50 equivalents) in CH_2Cl_2 at 25 °C.

Fig. S20 Reaction of $L_2Cu(O_2N)$ with excess of PPh_3 (25~50 equivalents) in CH_2Cl_2 at 25 °C.

Establishing Rate Law with $L_1Cu(O_2N)$ or $L_2Cu(O_2N)$: The following stock solutions were prepared at 25 °C between experiments: 2.0 mM $L_1Cu(O_2N)$ or $L_2Cu(O_2N)$ and 20.0 mM PPh_3 in dichloromethane. Reactions were conducted in a UV-Vis cuvette: 2 mL of the copper solution was transferred to a cuvette under nitrogen environment

and sealed with a septum which maintained a steady dark brown color. 0.12 – 0.25 mL (25, 30, 40, 45 and 50 eq.) of the phosphine solution was drawn into a syringe also under nitrogen environment. The cuvette was placed in the UV-

vis at temperature 25 °C. The solution was allowed to stir for ~3 min to allow the temperature to be uniform. After ~30 s collection the phosphine solution was injected. The drop of the peak at ~780 nm ($L_1Cu(O_2N)$) and ~871 nm ($L_2Cu(O_2N)$) was followed after the injection of the phosphine solution. The final color of the solution was yellow.
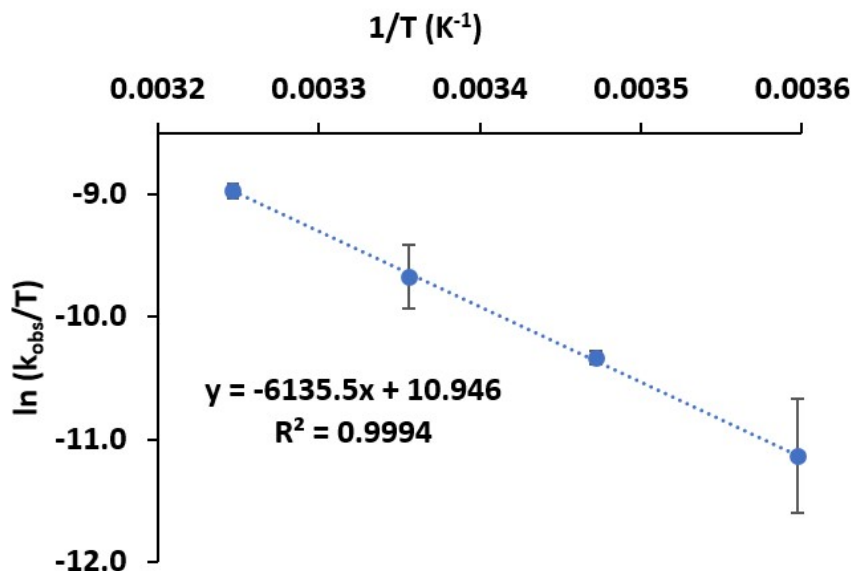
Fig. S21 Eyring plot for the reaction of $L_1Cu(O_2N)$ with two equivalents of PPh_3.

Erying analysis of copper(II) nitrite complexes: The following stock solutions were prepared at 25 °C between experiments: 2.0 mM $L_1Cu(O_2N)$ or $L_2Cu(O_2N)$ and 4.0 mM PPh_3 in dichloromethane. Reactions were conducted in a UV-Vis cuvette: 2 mL of the copper solution was transferred to a cuvette inside the glove box and sealed with a septum which maintained a steady dark brown color that varied slightly with the different complexes. 0.1 mL (2 eq.) of the phosphine solution was drawn into a syringe inside the glove box as well. The cuvette was placed in the UV-vis equipped with the cryostat set to maintain the temperature. The solution was allowed to stir for ~5 min to allow the temperature to be uniform. After ~30 s collection the phosphine was injected. The drop of the peak at ~780 nm ($L_1Cu(O_2N)$) and 871 nm ($L_2Cu(O_2N)$) were followed after the injection of the phosphine solution. The final color of the solution was yellow. For $L_1Cu(O_2N)$ and $L_2Cu(O_2N)$ the temperatures used were 278-308 K. Plotting the ln(k/T) as function of 1/T according to the Eyring equation yielded activation enthalpy and activation entropy.
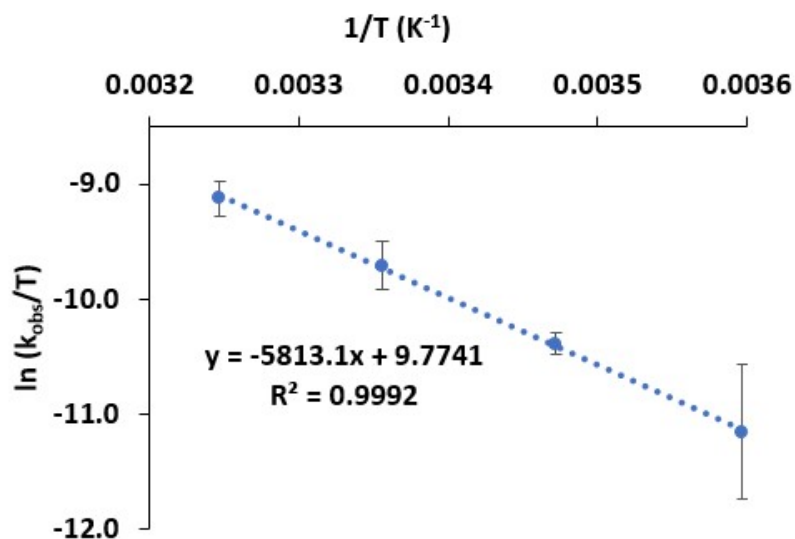
Fig. S22 Eyring plot for the reaction of $L_2Cu(O_2N)$ with two equivalents of PPh$_3$.

Calculation of the Activation Parameters:[3] The Eyring plot for each compound allows for the use of the Eyring equation:

$$ln\frac{k}{T} = \frac{-\Delta H^{\ddagger}}{T} \cdot \frac{1}{T} + ln\frac{k_B}{h} + \frac{-\Delta S^{\ddagger}}{R}$$

to calculate the activation parameters, where k is the rate constant (M^{-1}s^{-1}), T is the temperature (K), $\Delta H^{\ddagger}$ is the enthalpy of activation (J/mol), R is the gas constant (J/K•mol), k$_B$ is the Boltzmann constant (J/K), h is the Planck constant (J•s), and $\Delta S^{\ddagger}$ is the entropy of activation (J/mol•K). The equation of the line from the Eyring plot fits the form of the equation such that the slope of the line is equal to -$\Delta H^{\ddagger}$/R and the intercept of the line is equal

to $\Delta S^{\ddagger}/R$ - $ln\dfrac{k_B}{h}$. The values for $\Delta H^{\ddagger}$ and $\Delta S^{\ddagger}$ were then converted to kcal/mol and cal/mol•K respectively. To calculate the Gibbs free energy of activation ($-\Delta G^{\ddagger}$) at 298 K the equation:

$$\Delta G^{\ddagger} = \Delta H^{\ddagger} - T\Delta S^{\ddagger}$$

was used with T = 298 K. The standard error in the slope and intercept were calculated using the Microsoft Excel linest function and carried through the calculations to arrive at the errors in the activation parameters.

Table S1 The experimental and calculated metric parameters of $\mathbf{L_1}$CuCl and $\mathbf{L_2}$CuCl.

	Cu-N$_{1(py)}$	Cu-N$_2$	Cu-N$_3$	Cu–Cl	N$_1$–Cu–N$_3$	N$_2$–Cu–Cl	τ_4
Exp-$\mathbf{L_1}$CuCl	2.044	1.969	1.940	2.251	169.4	167.4	0.164
Exp-$\mathbf{L_2}$CuCl	2.020	1.938	1.931	2.236	148.1	146.6	0.463
DFT-$\mathbf{L_1}$CuCl	2.072	1.963	1.973	2.255	162.0	160.6	0.265
DFT-$\mathbf{L_2}$CuCl	2.066	1.972	1.965	2.256	147.6	148.7	0.451

Table S2 The overlap population analysis between Cu and coordinated donor atoms for the β-LUMOs of $\mathbf{L_1}$CuCl and $\mathbf{L_2}$CuCl.

	Cu–Cl	Cu–N$_{1(py)}$	Cu–N$_{\mathbf{L1/L2}}$	Orbital energy (eV)
β-LUMO of $\mathbf{L_1}$CuCl	-0.052	-0.078	-0.132	-2.466
β-LUMO of $\mathbf{L_2}$CuCl	-0.045	-0.053	-0.117	-2.534

Table S3 First order rate constants for reaction of copper(II) nitrito complexes (2 mM) with triphenylphosphine (4 mM) in CH_2Cl_2 at 278-308 K.

	k_{obs} (s^{-1})	
Temperature (K)	$\mathbf{L_1}$Cu(O$_2$N)	$\mathbf{L_2}$Cu(O$_2$N)
278	$(4.06 \pm 0.47) \times 10^{-3}$	$(3.97 \pm 0.11) \times 10^{-3}$
288	$(9.39 \pm 0.05) \times 10^{-3}$	$(8.85 \pm 0.25) \times 10^{-3}$
298	$(1.89 \pm 0.26) \times 10^{-2}$	$(1.81 \pm 0.48) \times 10^{-2}$
308	$(3.93 \pm 0.05) \times 10^{-2}$	$(3.36 \pm 0.42) \times 10^{-2}$
$\Delta H^{\ddagger}$ (kcal mol^{-1})	12.19 ± 0.14	11.55 ± 0.16
$\Delta S^{\ddagger}$ (cal K^{-1} mol^{-1})	-78.24 ± 2.61	-69.86 ± 1.46
$\Delta G^{\ddagger}$ (kcal mol^{-1})	18.67 ± 1.04	16.94 ± 0.34

Table S4. Values of $E_{1/2}$ for Cu(II) complexes.

Complexes	E_a	E_c	$E_{1/2}(V)$	$\Delta E(V)$	ref
$L_ACu(O_2N)^c$	-0.370	-0.470	-0.420	0.099	4
$L_BCu(O_2N)^b$	-0.046	-0.179	-0.113	0.133	3
L₁$CuCl^a$	-0.092	-0.240	-0.166	0.148	this work
L₂$CuCl^a$	+0.140	-0.032	-0.054	0.108	this work
L₃$CuCl^a$	-0.152	-0.362	-0.257	0.210	this work
L₄$CuCl^a$	+0.060	-0.142	-0.041	0.082	this work
L₁$Cu(O_2N)^a$	-0.099	-0.255	-0.177	0.156	this work
L₂$Cu(O_2N)^a$	+0.059	+0.194	+0.126	0.135	this work

[a] All values reported vs NHE, by adding 400 mV to the value measured vs the SCE couple in CH_3CN with Bu_4NPF_6 as electrolyte and potentials (in V vs. SCE) were measured at a glassy carbon electrode at a scan rate of 300 mVs⁻¹.

[b] L_B = (2,6-dimethyl)phenylamino-4-(2,6-dimethyl)phenyliminopent-2-ene. CV measured in THF using NHE as reference electrode.

[c] L_A = 1,1,1,5,5,5-Hexafluoro-2-(2,6-diisopropyl)phenylamino-4-(2,6-diisopropyl)phenyliminopent-2-ene. CV measured in THF using NHE as reference electrode.

Table S5. DFT optimized result: atomic coordinates of **L₁CuCl**.

Center Number	Atomic Number	Atomic Type	Coordinates (Angstroms)		
			X	Y	Z

Center Number	Atomic Number	Atomic Type	X	Y	Z
1	29	0	-0.83963	0.01529	-0.38958
2	17	0	-0.05210	-1.73376	-1.57516
3	7	0	-2.74219	-0.80375	-0.36365
4	7	0	-1.85366	1.63088	0.07573
5	7	0	0.89180	0.75968	0.19564
6	6	0	-3.05219	-2.09678	-0.51371
7	6	0	-4.36142	-2.54615	-0.48397
8	6	0	-5.38079	-1.61421	-0.30800
9	6	0	-5.05359	-0.27564	-0.16038
10	6	0	-3.71128	0.09532	-0.18771
11	6	0	-3.28724	1.52363	-0.03019
12	6	0	-2.21365	3.97912	0.67287
13	6	0	-1.32124	2.78586	0.45366
14	6	0	0.03892	2.96325	0.70044
15	6	0	1.05254	1.98917	0.65170
16	6	0	2.37947	2.40062	1.23887
17	6	0	0.19287	-2.05645	2.38223
18	6	0	1.85214	-0.94838	3.90360
19	6	0	1.18986	-0.90588	2.52963
20	6	0	2.18315	-0.93265	1.38464
21	6	0	3.26954	-1.80587	1.41970
22	6	0	4.16135	-1.88125	0.35870
23	6	0	3.96186	-1.09300	-0.76637
24	6	0	3.66427	1.74939	-2.22178
25	6	0	2.74887	-0.27186	-3.37760
26	6	0	2.66888	0.59240	-2.12095

27	6	0	2.87824	-0.22016	-0.85788
28	6	0	2.00436	-0.13381	0.24101
29	1	0	-2.20214	-2.75784	-0.67916
30	1	0	-4.57454	-3.60507	-0.60308
31	1	0	-6.42200	-1.93092	-0.28513
32	1	0	-5.82044	0.48517	-0.02087
33	1	0	-3.80674	1.93472	0.85417
34	1	0	-3.67962	2.09340	-0.89521
35	1	0	-2.84280	4.17684	-0.20562
36	1	0	-2.89183	3.82112	1.52356
37	1	0	-1.62565	4.87806	0.87894
38	1	0	0.34105	3.95032	1.04082
39	1	0	2.44983	3.48923	1.33049
40	1	0	2.48123	1.97019	2.24612
41	1	0	3.23099	2.03111	0.65867
42	1	0	0.71189	-3.02393	2.44766
43	1	0	-0.56845	-2.02294	3.17464
44	1	0	-0.31162	-2.02857	1.40520
45	1	0	2.61651	-0.16689	4.01289
46	1	0	1.10187	-0.80546	4.69307
47	1	0	2.33731	-1.91600	4.09416
48	1	0	0.62020	0.03417	2.46837
49	1	0	3.42120	-2.43971	2.29361
50	1	0	5.00934	-2.56316	0.40486
51	1	0	4.65709	-1.16820	-1.60286
52	1	0	3.51691	2.30388	-3.15909
53	1	0	3.56184	2.46448	-1.39475
54	1	0	4.69923	1.37643	-2.21533
55	1	0	2.06815	-1.12845	-3.30745
56	1	0	2.47121	0.32122	-4.25990
57	1	0	3.76823	-0.64737	-3.54896

| 58 | 1 | 0 | 1.65545 | 1.01688 | -2.07951 |

Table S6. DFT optimized result: atomic coordinates of **L₂CuCl**.

Center Number	Atomic Number	Atomic Type	Coordinates (Angstroms)		
			X	Y	Z
1	29	0	0.77276	0.21291	-0.25735
2	17	0	0.22506	-1.10614	-2.00367
3	7	0	2.63899	-0.67237	-0.21485
4	7	0	1.54045	1.90551	0.40098
5	7	0	-0.96739	0.45771	0.62137
6	6	0	2.81239	-1.92295	0.21207
7	6	0	4.04622	-2.55387	0.17369
8	6	0	5.12723	-1.85148	-0.34668
9	6	0	4.93596	-0.55589	-0.80739
10	6	0	3.66581	0.01087	-0.73284
11	6	0	3.35610	1.39317	-1.21249
12	6	0	2.84687	2.30021	-0.09644
13	6	0	1.75927	3.77492	1.96895
14	6	0	1.00822	2.60174	1.39440
15	6	0	-0.24254	2.32670	1.96200
16	6	0	-1.18156	1.36432	1.56060
17	6	0	-2.52326	1.42118	2.24553
18	6	0	-2.31945	1.60883	-2.72380
19	6	0	-4.13633	2.44015	-1.20394
20	6	0	-2.83702	1.64144	-1.28563
21	6	0	-2.98157	0.22987	-0.75124

22	6	0	-4.02177	-0.57518	-1.21289
23	6	0	-4.15418	-1.89266	-0.79660
24	6	0	-3.22371	-2.43218	0.07993
25	6	0	-1.72713	-2.55980	2.86686
26	6	0	-0.56819	-3.59372	0.88730
27	6	0	-1.13919	-2.30706	1.47979
28	6	0	-2.15604	-1.67223	0.55463
29	6	0	-2.05657	-0.32871	0.15177
30	1	0	1.92012	-2.42830	0.58303
31	1	0	4.14897	-3.57425	0.53298
32	1	0	6.11146	-2.31325	-0.40068
33	1	0	5.75678	0.01728	-1.23425
34	1	0	4.25543	1.84355	-1.65296
35	1	0	2.59695	1.33104	-2.00952
36	1	0	2.80410	3.32716	-0.49800
37	1	0	3.60228	2.31246	0.71126
38	1	0	1.19009	4.25536	2.76980
39	1	0	2.73054	3.46737	2.38041
40	1	0	1.96641	4.53216	1.20038
41	1	0	-0.55285	2.98215	2.77201
42	1	0	-2.91428	0.41791	2.45292
43	1	0	-2.45989	1.98378	3.18268
44	1	0	-3.26379	1.91875	1.60393
45	1	0	-2.16439	2.62879	-3.10379
46	1	0	-1.37468	1.05430	-2.79060
47	1	0	-3.04316	1.10942	-3.38445
48	1	0	-4.90399	2.03539	-1.87841
49	1	0	-4.55968	2.44321	-0.18951
50	1	0	-3.96272	3.48282	-1.50292
51	1	0	-2.08332	2.16839	-0.68140
52	1	0	-4.74086	-0.16345	-1.92172

53	1	0	-4.97761	-2.50284	-1.16492
54	1	0	-3.32284	-3.47155	0.39517
55	1	0	-2.58466	-3.24591	2.81008
56	1	0	-0.98050	-3.01275	3.53439
57	1	0	-2.07690	-1.62936	3.33479
58	1	0	-0.17922	-3.41793	-0.12552
59	1	0	0.24083	-3.98503	1.52304
60	1	0	-1.32991	-4.38327	0.82053
61	1	0	-0.30654	-1.59546	1.59883

References:

1. Maji, R. C.; Barman, S. K.; Roy, S.; Chatterjee, S. K.; Bowles, F. L.; Olmstead, M. M.; Patra, A. K., Copper complexes relevant to the catalytic cycle of copper nitrite reductase: electrochemical detection of NO (g) evolution and flipping of NO_2 binding mode upon $Cu^{II} \rightarrow Cu^{I}$ reduction. *Inorg. Chem.* **2013,** *52*, 11084-11095.

2. Chandra Maji, R.; Mishra, S.; Bhandari, A.; Singh, R.; Olmstead, M. M.; Patra, A. K., A Copper (II) Nitrite That Exhibits Change of Nitrite Binding Mode and Formation of Copper (II) Nitrosyl Prior to Nitric Oxide Evolution. *Inorg. Chem.* **2018,** *57*, 1550-1561.

3. Stauffer, M.; Sakhaei, Z.; Greene, C.; Ghosh, P.; Bertke, J. A.; Warren, T. H., Mechanism of O-Atom Transfer from Nitrite: Nitric Oxide Release at Copper(II). *Inorg. Chem.* **2021,** *60*, 15968–15974.

4. Sakhaei, Z.; Kundu, S.; Donnelly, J. M.; Bertke, J. A.; Kim, W. Y.; Warren, T. H., Nitric oxide release via oxygen atom transfer from nitrite at copper (II). *Chem. Commun.* **2017,** *53*, 549-552.

5. Sanders, B. C.; Hassan, S. M.; Harrop, T. C., NO_2^- Activation and Reduction to NO by a Nonheme $Fe(NO_2)_2$ Complex. *J. Am. Chem. Soc.* **2014,** *136*, 10230-10233.

6. Kumar, M.; Dixon, N. A.; Merkle, A. C.; Zeller, M.; Lehnert, N.; Papish, E. T., Hydrotris(triazolyl)borate Complexes as Functional Models for Cu Nitrite Reductase: The Electronic Influence of Distal Nitrogens. *Inorg. Chem.* **2012,** *51*, 7004-7006.

7. Cioncoloni, G.; Roger, I.; Wheatley, P. S.; Wilson, C.; Morris, R. E.; Sproules, S.; Symes, M. D., Proton-coupled electron transfer enhances the electrocatalytic reduction of nitrite to NO in a bioinspired copper complex. *ACS Catal* **2018,** *8*, 5070-5084.